

---

# Magneto-optical imaging of magnetic deflagration in $\text{Mn}_{12}$ -Acetate

D. VILLUENDAS<sup>1</sup>, D. GHEORGHE<sup>2</sup>, A. HERNÁNDEZ-MÍNGUEZ<sup>1</sup>, F. MACIÀ<sup>1</sup>, J. M. HERNANDEZ<sup>1</sup>, J. TEJADA<sup>1</sup> and R. J. WIJNGAARDEN<sup>2</sup>

<sup>1</sup> *Departament de Física Fonamental, Facultat de Física, Universitat de Barcelona - Avda. Diagonal 647, Planta 4, Edifici Nou, 08028 Barcelona, Spain*

<sup>2</sup> *Faculty of Sciences, Division of Physics and Astronomy, Vrije Universiteit - De Boelelaan 1081, 1081 HV Amsterdam, The Netherlands*

PACS 75.50.Xx – Molecular magnets

PACS 75.60.Jk – Magnetization reversal mechanism

PACS 85.70.Sq – Third pacs description

**Abstract.** - For the first time, we explore the morphology and dynamics of spin avalanches in  $\text{Mn}_{12}$ -Acetate crystals using magneto-optical imaging. We observe an inhomogeneous relaxation of the magnetization, the spins reversing first at one edge of the crystal and a few milliseconds later at the other end. Our data fit well with the theory of magnetic deflagration, demonstrating that very slow deflagration rates can be obtained, which makes new types of experiments possible.

---

Synthesized in 1980,  $\text{Mn}_{12}$ -Acetate is a crystal composed of a large number (typically of the order of  $10^{17}$ ) of  $[\text{Mn}_{12}\text{O}_{12}(\text{CH}_3\text{COO})_{16}\cdot(\text{H}_2\text{O})_4]\cdot 2\text{CH}_3\text{COOH}\cdot 4\text{H}_2\text{O}$  molecules, each with a large spin  $S = 10 \mu_B$  [1]. Its mono-disperse structure, strong spin anisotropy as well as the hysteretic behavior at low temperatures [2] have attracted a lot of interest. From a fundamental point of view,  $\text{Mn}_{12}$ -Acetate offers a unique playground to study phenomena at the frontier between classical and quantum mechanics, whereas from the point of view of applications, it offers an interesting perspective towards 3D high-density magnetic storage devices [3]. These possibilities motivated many studies on the magnetic properties of these molecular crystals (see refs. [4–6] for reviews). The strong uniaxial anisotropy accounts for the doubly-degenerate potential well, shown in fig.1(a). Each well is characterized by a discrete distribution of energetic levels, corresponding to different projections  $m$  ( $m = \pm 10, \pm 9, \dots, 0$ ) of the total spin along the easy anisotropy axis ( $c$ -axis). In such a system, the relaxation of the magnetization can proceed via three mechanisms: thermal relaxation, quantum tunnelling and avalanches. Thermal relaxation occurs when the thermal excitations are strong enough to promote the spins over the potential barrier. When this condition is not fulfilled, the effect of the thermal energy is simply to populate the upper levels of the potential well, thus increasing the propensity

for spin tunnelling through the anisotropy barrier [7]. Quantum tunnelling effects appear irrespective of temperature, as steps in the hysteresis curve which occur systematically at well defined externally applied magnetic fields, the so-called resonant fields  $H_{res}$  [8–10]. At  $H_{res}$  some energy levels in both wells are at equal energy.

Thermally induced relaxation processes are characterized by a long relaxation time  $\tau$ , typically of the order of a few hundred ms. Much shorter relaxation times, less than 1 ms [11–16], have been observed experimentally. Since in such cases the relaxation of the magnetization is typically accompanied by a significant heat release this effect is attributed to a thermal runaway or avalanche. It was observed that this spin reversal (avalanche) does not occur simultaneously for all the spins in the sample, but follows a domino effect, with spin reversal nucleation at one edge of the sample and subsequent propagation through the crystal over a narrow spin reversal front [12]. This type of relaxation is known as magnetic deflagration, due to its parallelism with the propagation of a chemical combustion along a burning substance. In the magnetic case, the role of the chemical energy is played by the Zeeman energy and the "ashes" are the spins that have already relaxed. The amount of heat released by the thermal runaway depends significantly on the experimental parameters (temperature, sweep rate of the magnetic field) [18]. However, up to now, no correlation was made between the external

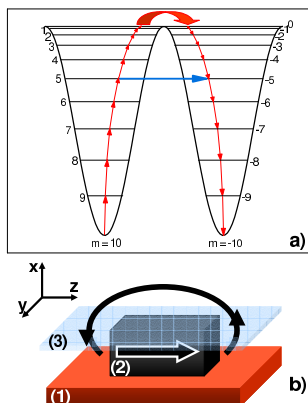


Fig. 1: (Color online) a) Doubly degenerate potential well of a  $\text{Mn}_{12}$ -Acetate crystal in zero applied magnetic field. The possible relaxation mechanisms are schematically indicated by the arrows: thermal relaxation (red arrows), in which the thermal energy promotes the spins above the potential barrier in the adjacent well, and quantum tunnelling (blue arrow), in which the spins thread through the energy barrier in the adjacent well. b) Schematic representation of the experimental configuration: (1) Cernox resistor, (2)  $\text{Mn}_{12}$ -Acetate crystal, (3) magneto-optically active layer (indicator).

parameters, the excitation energy and the morphology of the spin reversal fronts of the magnetic deflagration. In this study we set on providing an answer to this open question by using for the first time an optical technique: magneto-optical imaging. This technique allows the direct visualization of the overall magnetic field distribution at the surface of the sample as a grey-scale intensity image, the value of each grey level being proportional to the local value of the magnetic field component perpendicular to the surface of the sample [19] (i.e. the  $x$ -axis in fig.1(b)). A detailed description of our magneto-optical set-up can be found in ref. [20]. Our sample, a  $\text{Mn}_{12}$ -Acetate crystal of  $1.2 \times 0.5 \times 0.5 \text{ mm}^3$ , was mounted on a LakeShore Cernox Thermometer, model CX-1050BR, which we used as a heater. The sample was visualized using the Faraday effect in a  $5 \mu\text{m}$  Bi-substituted yttrium iron garnet (YIG) film with in-plane anisotropy [21] and a saturation field of 90 mT. The magneto-optically active layer was 'glued' on top of the  $\text{Mn}_{12}$  crystal with nanodecane ( $\text{C}_{19}\text{H}_{40}$ ), 99% purity. A schematic view of the experimental configuration is shown in fig.1(b). The ensemble was mounted on a home-built optical insert and placed in a commercial Oxford Instruments vector magnet. The system allows the generation of magnetic fields up to  $H_{max} = 1 \text{ T}$ , in any orientation relative to the sample, by simultaneous use of three superconducting coils. Since at low temperature an external field of 1 T is too small to ensure the saturation of the magnetization, we prepared the initial state of the sample as follows: we field cooled the crys-

tal in an applied magnetic field of 1 T, oriented along the anisotropy axis ( $z$ -axis in fig.1 (b)), through the blocking temperature  $T_B$  (above which thermal relaxation is the dominant relaxation mechanism) [4], down to the desired temperature  $T$ . Once  $T$  was reached, we decreased the externally applied magnetic field  $H$  from 1 T to a smaller value, indicated below, and anti-parallel with respect to the magnetic moment of the sample. Subsequently, voltage pulses of 10 V and various duration  $t_p$  were applied to the Cernox resistor, using a Wavetek pulse generator. We performed two sets of experiments, which we will henceforth refer to as *experiment 1* ( $T = 1.5 \text{ K}$ ,  $H = -0.1 \text{ T}$ ,  $t_p = 10 \text{ ms}$ ) and *experiment 2* ( $T = 1.6 \text{ K}$ ,  $H = -0.45 \text{ T}$ ,  $t_p = [0.01, 10] \text{ ms}$ ), in which the initial state was prepared using different values for the external parameters, as indicated in the brackets. The magnetization reversal was filmed using a Teli CCD camera (model CS8320C) with an active area of  $752 \times 582$  pixels and a recording speed of 50 fields/second. The relatively low temporal resolution of our experiments motivated the use of small magnetic fields  $H$ , since a smaller  $H$  is known to lead to slower relaxation [22].

The results of *experiment 1* are shown in fig.2. Fig.2(1) corresponds to the initial state, prior to the application of the heat pulse. The sample has a strong in-plane magnetic moment which appears as the contrasting bright and dark regions at the upper and lower edges of the crystal. The bright region corresponds to a high positive magnetic field whereas the dark region to a high negative magnetic field. After the heat pulse (which yields an energy of  $50 \mu\text{J}$  [23]) is applied, a slow decrease of the contrast at the edges of the sample is initially observed (fig.2(2)). This corresponds to a decrease of the local magnetic fields, hence to a reduction of the in-plane magnetic moment of the sample. Subsequently, bright regions become clearly visible on the dark background at the lower edge of the sample, fig.2(3), where gradually, the field changes sign, fig.2(4). Clearly, the deflagration and its associated sign reversal of magnetization has started at the lower edge. The upper edge is still unaffected and remains in its original magnetization direction, see fig.2(5). Eventually, also the local magnetic field at the upper edge changes sign. The magnetization reversal gradually continues, until the magnetic moment of the sample has completely reversed, fig.2(6), (7) and (8). It can be noticed, by comparing fig.2(1) and fig.2(8), that the strength of stray field at the edges of the sample is much stronger prior to the application of the heat pulse. This is due to the fact that the magnetic moment relaxes toward the equilibrium state, which, for the values of  $H$  used in our experiments, is lower than the saturation magnetization: fig.2(1) is the magnetization induced by the external field of 1 T and fig.2(8) is the magnetization induced by 0.1 T only.

The relaxation process observed in our experiments is similar to the one reported in ref. [12] in the sense that the magnetization reversal nucleates first at the edge of the sample. Additionally, the relaxation starts systemat-

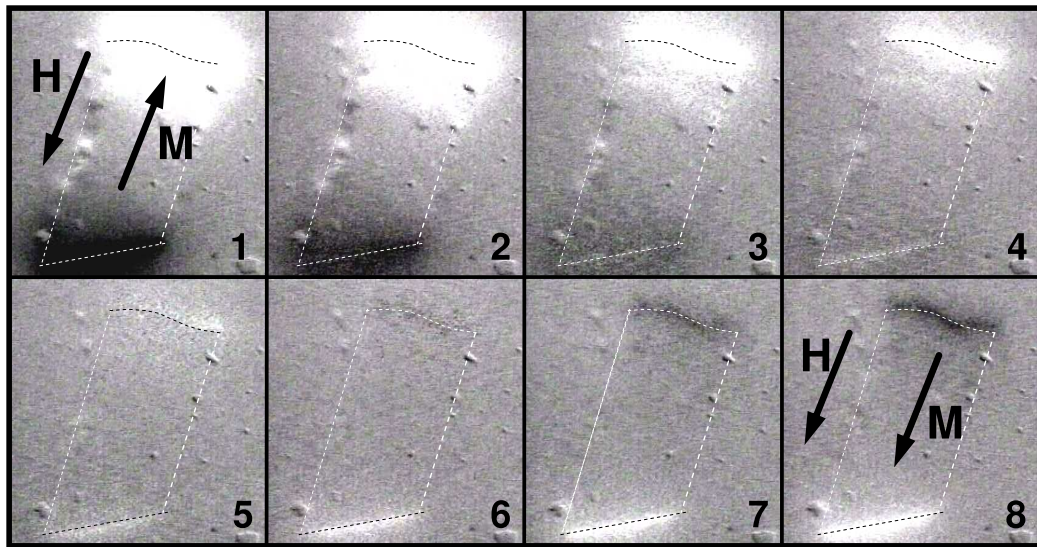


Fig. 2: Images showing the time evolution of the in-plane magnetic moment of the sample obtained in *experiment 1*. The image in fig.2(1) corresponds to the initial state, prior to the application of the heat pulse. All subsequent pictures were taken after the heat pulse. The time span between consecutive frames is 20 ms. The magnetization reversal nucleates at the lower edge of the sample and propagates, along the anisotropy axis, towards the upper edge of the crystal. The intensity of the gray-levels in the images is proportional to the intensity of the local magnetic field. The arrows indicate the orientations of the magnetic moment  $M$  and the externally applied field  $H$ . The contour of the sample is indicated by the dashed lines.

ically at the lower, sharper edge of the sample in all our measurements. This agrees well with the results reported in ref. [16, 17], where it was observed that the deflagration front is ignited at the point of the crystal where the local magnetic field is highest. In our case, the demagnetizing field  $H_d$  is smaller at the sharper edge, which implies that irrespective of the sign of the applied field  $H$ , the total magnetic field ( $H + H_d$ ) at this edge is highest. However, by contrast to the results of ref. [12], no gradual propagation of the spin reversal, over a narrow front along the width of the sample, was observed in our experiments. Furthermore, the time span for complete relaxation is larger in our experiment as compared to ref. [12] and, at first sight one could imagine that we are observing conventional thermal relaxation, induced by the heater.

To try to understand the differences between our experimental results and the data of ref. [12], we modified our experimental conditions as detailed above for *experiment 2*. This was done in order to reduce the anisotropy barrier and probe the avalanche nucleation at very small thermal excitations. The time span  $t_p$  over which the heat pulses were applied were logarithmically increased from 0.01 ms to 10 ms. For very short time pulses,  $t_p = 0.01$  ms (equivalent energy 50 nJ), we observed no relaxation of the magnetic moment, indicating that in this case the excitation energy is too small to promote the magnetization reversal. In all other experiments, corresponding to  $t_p = 0.1$  ms (0.5  $\mu$ J),  $t_p = 1$  ms (5  $\mu$ J) and  $t_p = 10$  ms (50  $\mu$ J) a complete reversal of the magnetic moment is observed, the relaxation mechanism following the same pattern as detailed for *experiment 1*. For each of these experiments we calculated the variation of the local field intensity at the edges of the crystal as a function of time. The results are shown in fig.3. The data from all three experiments collapse to the same curves, which can be fitted by an exponential law with  $\tau = 65.8$  ms. A relaxation time of  $\tau = 65.8$  ms implies through Arrhenius' law,  $\tau = \tau_0 \exp \frac{U(H)}{k_B T}$ , that the temperature of the sample, after the heat pulse, rises to  $T = U / \ln(\tau / \tau_0) \approx 4.5$  K (assuming that  $U = 59$  K when  $H_z = -0.45$  T [24]). **This value is higher than the blocking temperature  $T_B \simeq 3.5$  K (determined from DC magnetization measurements), hence thermal relaxation plays a role.** On the other hand, the mechanism cannot be simple thermal relaxation, since in that case the relaxation time would decrease with increasing  $t_p$ , in contrast to our experimental observations.

To solve this apparent contradiction we propose the following explanation: the externally applied heat pulse (provided that  $t_p > 0.1$  ms) triggers a deflagration wave. During the avalanche, the spin reversal is associated to an energy release in the sample equal to the Zeeman energy  $E_z = \mu_0 H \Delta M_z$ , where  $H$  is the applied magnetic field and  $\Delta M_z = N g \mu_B \Delta m$  is the change in the total magnetic moment of the sample due to the spins that have changed their projection from  $m = -10$  to  $m = 10$  (im-

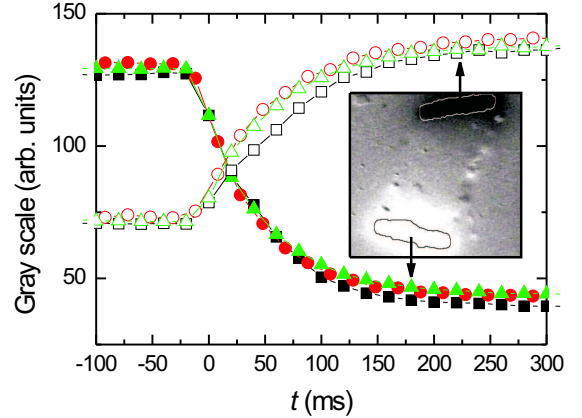


Fig. 3: (Color online) Time evolution of magneto-optical intensity at the upper and lower edges of the crystal for the three cases of *experiment 2*. The different symbols correspond to different excitation energies: 0.5  $\mu$ J (squares), 5  $\mu$ J (circles) and 50  $\mu$ J (triangles). The inset shows the regions over which the average intensity was calculated. All curves fit to an exponential law with a single  $\tau = 65.8$  ms.

plying  $\Delta m = 20$ ). The total number  $N$  of molecules in the sample can be easily evaluated using  $N = v \rho N_A / M$ , where  $N_A = 6.022 \cdot 10^{23} / \text{mol}$  is the Avogadro number, the volume  $v$  of the crystal is  $v = 1.2 \times 0.5 \times 0.5 = 0.3 \cdot 10^{-3} \text{ cm}^3$ , the density  $\rho = 1.84 \text{ g/cm}^3$  and the molecular mass  $M = 2060,3 \text{ g/mol}$ . Using  $g = 2$ , the calculation yields  $N = 1.6 \cdot 10^{17}$ ,  $\Delta M_z = 6.0 \cdot 10^{-5} \text{ J/T}$ , which amounts to a Zeeman energy  $E_z \simeq 30 \mu\text{J}$ . This energy is larger by a factor of 60 compared to the excitation energy ( $\sim 0.5 \mu\text{J}$ ) for which we already observe avalanches in our experiments. Since even for larger excitation pulses (up to 50  $\mu\text{J}$ ) the complete relaxation of the magnetic moment of the sample occurs over the same time interval, it is plausible to assume that, for the range of excitation energies used in our measurements, only a small fraction of the energy provided by the Cernox thermometer is transferred to the crystal. Hence, the increase in the temperature of the sample is mainly due to the Zeeman contribution, which is the same in our experiments, since the externally applied magnetic field (hence the distance between the energetic levels in the crystal) is the same. The heat produced by the deflagration wave is mostly released to the environment, such that the temperature of the crystal **does not significantly exceed  $T_B$** . This explains why we clearly observe the in-plane magnetic moment of the sample at any moment during the deflagration.

The temperature of the front of reversing spins in our sample is lower than in previously reported experiments, [12, 13] which implies a higher value of  $\tau$ , hence a slower relaxation, as we clearly observe in our measurements. We estimate that the speed of the front of reversing spins is of the order of  $v \approx 12 \text{ mm/s}$ , in contrast to some much higher values reported in the literature. [12–15].

Finally, the width of the region over which the simultaneous relaxation of the spins is expected to occur can be easily estimated using  $l_D = \sqrt{\kappa\tau}$  [12, 22]. From the literature [25] it is known that  $\kappa$  for Mn<sub>12</sub> is in the range of  $10^{-5} - 10^{-4}$  m<sup>2</sup>/s hence  $l_D \approx 0.8 - 2.5$  mm. This is of the order of the length of our sample, which also explains why we have not seen the narrow front of reversing spins reported in ref. [12].

In conclusion we have visualized the magnetic deflagration using for the first time an optical technique. We have shown that depending on the environment and the size of the sample, it is possible to ignite deflagrations with long combustion times and wide magnetization fronts. We show that a reduction of the propagation speed of magnetic deflagrations is experimentally accessible, which opens the possibility of new types of experiments.

\* \* \*

This work was supported by FOM (Stichting voor Fundamenteel Onderzoek der Materie) that is financially supported by NWO (Nederlandse Organisatie voor Wetenschappelijk Onderzoek) and the Spanish Ministerio de Educación y Ciencia (MEyC), contract MAT2005-06162. A.H.-M. and F.M. thank the MEyC for a research grant. J.M.H. thanks the MEyC and University of Barcelona for a Ramón y Cajal research contract.

## REFERENCES

- [1] LIS T., *Acta Cryst. B*, **36** (1980) 2024.
- [2] SESSOLI R. and GATTESCHI D. and CANESCHI A. and NOVAK M. A., *Nature*, **365** (1993) 141.
- [3] SRAJER G. and LEWIS L.H. and BADER S.D. and EPSTEIN A.J. and FADLEY C.S. and FULLERTON E.E. and HOFFMAN A. and KORTRIGHT J.B. and KRISHNAN K.M. and MAJETICH S.A. and RAHMAN T.S. and ROSS C.A. and SALAMON M.B. and SHULLER I.K. and SCGHULTNESS T.C. and SUN J.Z., *J. Magn. Magn. Mat.*, **307** (2006) 1.
- [4] FRIEDMAN J. R., *Exploring the Quantum/Classical Frontier: Recent Advances in Macroscopic Quantum Phenomena*, edited by FRIEDMAN J. R. and HAN S. (Nova Science, Hauppauge, NY) 2003, p. 179.
- [5] GATTESCHI D. and SESSOLI R., *Angew. Chem., Int. Ed.*, **42** (2003) 268-297.
- [6] DEL BARCO E. and KENT A. D. and HILL S. and NORTH J. M. and DALAL N. S. and RUMBERGER E. and HENDRIKSON D. N. and CHAKOV N. and CHRISTOU G., *J. Low Temp. Phys.*, **140** (2005) 119-174.
- [7] CHUDNOVSKY E. M. and TEJADA J., *Macroscopic Quantum Tunneling of the Magnetic Moment* (Cambridge University Press, Cambridge) 1998.
- [8] FRIEDMAN J. R. and SARACHIK M. P. and TEJADA J. and ZIOLO R., *Phys. Rev. Lett.*, **76** (1996) 3830-3833.
- [9] HERNÁNDEZ J. M. and ZHANG X. X. and LUIS F. and BARTOLOMÉ J. and TEJADA J. and ZIOLO R., *Europhys. Lett.*, **35** (1996) 301-306.
- [10] HERNANDEZ J. M. and ZHANG X. X. and LUIS F. and TEJADA J. and FRIEDMAN J. R. and SARACHIK M. P. and ZIOLO R., *Phys. Rev. B*, **55** (1997) 5858-5865.
- [11] PAULSEN C. and PARK J. G., *Quantum Tunneling of Magnetization-QTM'94*, edited by GUNTHER L. and BARBARA B. (Kluwer, Dordrecht, The Netherlands) 1995, p. 189-207.
- [12] SUZUKI Y. and SARACHIK M.P. and CHUDNOVSKY E.M. and MCHUGH S. and GONZALEZ-RUBIO R. and AVRAHAM N. and MYASOEDOV Y. and ZELDOV E. and SHTRIKMAN H. and CHAKOV N.E. and CHRISTOU G., *Phys. Rev. Lett.*, **95** (2005) 147201.
- [13] HERNÁNDEZ-MÍNGUEZ A. and HERNANDEZ J. M. and MACIÀ F. and GARCÍA-SANTIAGO A. and TEJADA J. and SANTOS P.V., *Phys. Rev. Lett.*, **95** (2005) 217205.
- [14] HERNÁNDEZ-MÍNGUEZ A. and MACIÀ F. and HERNANDEZ J. M. and TEJADA J. and SANTOS P.V., *J. Magn. Magn. Mater.*, **320** (2008) 1457-1463.
- [15] MCHUGH S. and JAAFAR R. and SARACHIK M. P. and MYASOEDOV Y. and FINKLER A. and SHTRIKMAN H. and ZELDOV E. and BAGAI R. and CHRISTOU G., *Phys. Rev. B*, **76** (2007) 172410.
- [16] HERNÁNDEZ-MÍNGUEZ A. and MACIÀ F. and HERNANDEZ J. M. and TEJADA J. and HE L. H. and WANG F. F., *Europhys. Lett.*, **75** (2006) 811-817.
- [17] JAAFAR REEM and MCHUGH S. and SUZUKI YOKO and SARACHIK M.P. and MYASOEDOV Y. and ZELDOV E. and SHTRIKMAN H. and BAGAI R. and CHRISTOU G., *J. Magn. Magn. Mater.*, **320** (2008) 695-698.
- [18] DEL BARCO E. and HERNANDEZ J. M. and SALES M. and TEJADA J. and RAKOTO H. and BROTO J. M. and CHUDNOVSKY E.M., *Phys. Rev. B*, **60** (1999) 11898-11901.
- [19] KOBLSCHKA M. R. and WIJNGAARDEN R. J., *Supercond. Sci. Technol.*, **8** (1995) 199.
- [20] WIJNGAARDEN R. J. and HEECK K. and WELLING M. and LIMBURG R. and PANNETIER M. and VAN ZETTEN K. and ROORDA V. L. G. and VOORWINDEN A. R., *Rev. Sci. Instrum.*, **72** (2001) 2661.
- [21] DOROSINSKII L. A. and INDENBOM M. V. and NIKITENKO V. I. and OSSIP'YAN YU. A. and POLYANSKII A. A. and VLASKO-VLASOV V. K., *Physica C*, **203** (1992) 149.
- [22] GARANIN D. A. and CHUDNOVSKY E. M., *Phys. Rev. B*, **76** (2007) 054410.
- [23] Note: over the range of temperatures at which we performed our experiments, the resistance of the Cernox Thermometer is  $R = 20$  k $\Omega$ , as specified by the manufacturer. The Joules energy dissipated due to the applied voltage pulses  $V$  was calculated using  $E_J = V^2 t_p / R$ .
- [24] HERNANDEZ J. M. and ZHANG X. X. and LUIS F. and BARTOLOME J. and TEJADA J. and ZIOLO R., *Europhys. Lett.*, **35** (1996) 301-306.
- [25] HERNANDEZ J. M. and SANTOS P. V. and MACIÀ F. and GARCÍA-SANTIAGO A. and TEJADA J., *Appl. Phys. Lett.*, **88** (2006) 012503.